# Molecular BioSystems

Accepted Manuscript


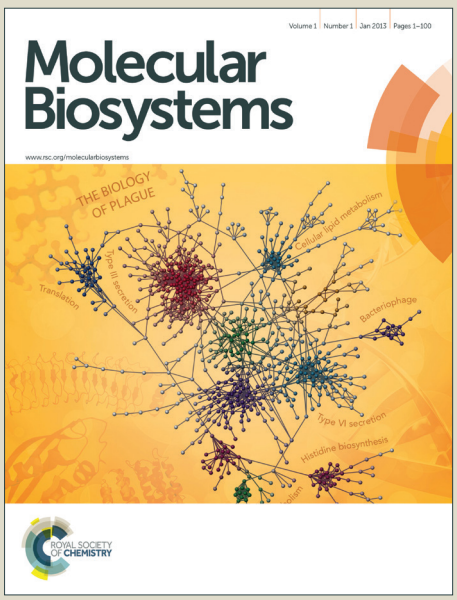


This is an *Accepted Manuscript*, which has been through the Royal Society of Chemistry peer review process and has been accepted for publication.

*Accepted Manuscripts* are published online shortly after acceptance, before technical editing, formatting and proof reading. Using this free service, authors can make their results available to the community, in citable form, before we publish the edited article. We will replace this *Accepted Manuscript* with the edited and formatted *Advance Article* as soon as it is available.

You can find more information about *Accepted Manuscripts* in the Information for Authors.




ROYAL SOCIETY OF CHEMISTRY

www.rsc.org/molecularbiosystems

# Metabolic flux pattern of glucose utilization by the phytopathogen and xanthan-producer *Xanthomonas campestris* pv. campestris: prevalent role of the Entner-Doudoroff pathway and minor fluxes through the pentose phosphate pathway and through glycolysis

Sarah Schatschneider [a,†], Claudia Huber [b], Heiko Neuweger [c,#], Tony Francis Watt [a], Alfred Pühler [d], Wolfgang Eisenreich [b], Christoph Wittmann [e], Karsten Niehaus [a], Frank-Jörg Vorhölter [a,d,*]

Authors addresses:

[a]) Abteilung für Proteom- und Metabolomforschung, Fakultät für Biologie, Universität Bielefeld, Bielefeld, Germany

[b]) Lehrstuhl für Biochemie, Center of Isotopologue Profiling, Technische Universität München, Garching, Germany

[c]) Computational Genomics, Centrum für Biotechnology (CeBiTec), Universität Bielefeld, Germany

[d]) Institut für Genomforschung und Systembiologie, Centrum für Biotechnology (CeBiTec), Universität Bielefeld, Bielefeld, Germany

[e]) Institut für Systembiotechnologie, Universität des Saarlandes, Saarbrücken, Germany

[†]) present address: School of Pharmacy, Boots Science Building, University of Nottingham, University Park, Nottingham, NG7 2RD, United Kingdom

[#]) present address: Bruker Daltonik GmbH, Bremen, Germany

*) Corresponding author. Office phone: +49-521-106-8701, Fax: +49-521-106-89041. E-mail: frank@CeBiTec.Uni-Bielefeld.DE

## Abstract

The well-studied plant pathogenic bacterium *Xanthomonas campestris* pv. campestris (Xcc) synthesizes the biotechnologically important polysaccharide xanthan gum, which is also regarded as a virulence factor in plant interactions. In Xcc, sugars like glucose are utilized as a source to generate energy and biomass for growth and pathogenicity. In this study, we used [1-$^{13}$C]glucose as a tracer to analyze the fluxes in the central metabolism of the bacterium growing in a minimal medium. $^{13}$C-Metabolic flux analysis based on gas chromatography–mass spectrometry (GC-MS) confirmed a prevalent catabolic role of the Entner-Doudoroff pathway. Comparative nuclear magnetic resonance (NMR)-based isotopologue profiling of a mutant deficient in glycolysis gave evidence for a moderate flux *via* glycolysis in the wild-type. In addition to reconfirming the Entner-Doudoroff pathway as catabolic main route, this approach affirmed a numerically minor but important flux *via* the pentose phosphate pathway.



## Keywords

$^{13}$C-labeling experiment, isotopomers, MFA, *Xanthomonadaceae*, central carbohydrate metabolism, catabolism

## Introduction

Gram negative bacteria of the genus *Xanthomonas* are plant pathogens that cause substantial losses in many crop plants like rice and citrus plants [1]. The γ-proteobacterium *Xanthomonas campestris pv.* campestris (Xcc) is the causal agent of the black rot disease of crucifers including the model plant *Arabidopsis thaliana* [2]. Like many other xanthomonads, Xcc spreads in the xylem before affecting other tissues of its host plants. Xcc synthesizes an exopolysaccharide termed xanthan gum that is a common feature of the genus *Xanthomonas* and assumed to have a role in plant pathogenicity [3–5]. Xanthan is produced biotechnologically and used widely as a thickener in the food, cosmetics, and oil drilling industries [6], usually by large-scale fed-batch cultivation of Xcc [7,8]. The production of xanthan gum increased significantly during the last years. In 2008, the worldwide consumption of xanthan gum was assumed to be 90,000 tons [9]. Knowing the metabolic fluxes that provide the hexose phosphate precursors of the polysaccharide is important to better understand the role of xanthan biosynthesis in plant infection and to further improve the yields in xanthan production.

Sugars like glucose are used as major carbon sources for Xcc fermentation [9]. To import and activate glucose, at least two pathways exist in Xcc. Either, glucose can be imported directly followed by phosphorylation by a glucokinase (EC 2.7.1.2) [10] generating glucose 6-phosphate, or glucose is metabolized *via* a periplasmic oxidative pathway [11]. However, this periplasmic pathway was assumed to play a minor role in Xcc [12] and hence was not in the focus of this study. *Via* both routes, glucose is finally converted into 6-phosphogluconate, which can be further metabolized *via* the pentose phosphate (PP) pathway or *via* the prevalent Entner-Doudoroff (ED) pathway [13,14]. Glyceraldehyde 3-phosphate delivered by these pathways can be further converted *via* the Embden-Meyerhof-Parnas pathway (EMP; glycolysis) [12]. Alternatively, glyceraldehyde 3-phosphate resulting from activity of ED pathway enzymes could enter a "hexose cycle", in which it is used to re-synthesize glucose 6-phosphate *via* the gluconeogenic activities of fructose-bisphosphate aldolase (EC 4.1.2.13), fructose 1,6-bisphosphatase (EC 3.1.3.11), and glucose 6-phosphate isomerase (EC 5.3.1.9) [15,16]. The *Xanthomonas* EMP pathway appeared to be incomplete in several studies as no activity was observed for the key enzyme phosphofructokinase (PFK) [11,17,18]. In contrast, a functional analysis of the Xcc genome [19] revealed the presence of a conserved *pfkA* gene similar to genes coding for phosphofructokinases. The product of this gene was recently identified as a pyrophosphate-dependent PFK which is conserved in other xanthomonads [20].

On the basis of Xcc B100 genome data [19], a large-scale model was established of the Xcc metabolism and applied for flux balance analysis (FBA) [21], thereby exceeding in scope a pioneering FBA model established previous to the availability of *Xanthomonas* genome data [12]. The large-scale FBA model [21] comprised 352 genes and 437 biochemical reactions including the PP pathway, the ED pathway, the EMP pathway, amino acid biosynthetic pathways, amino sugar and nucleotide sugar metabolism, fatty acid biosynthesis, lipopolysaccharide biosynthesis, nitrogen and sulfur metabolism, as well as peptidoglycan biosynthesis, glycogen biosynthesis, and carbohydrate uptake systems for glucose, gluconate, fructose, sucrose, mannose, galactose, and *N*-acetylglucosamine. FBA based on this model facilitated the prediction of individual flux rates for all individual reactions covered by the model. This metabolic network was holistically validated by appropriate experiments that included growth analysis on different carbon sources and phenotypic analyses of deletion mutants [21]. However, such a validation can provide no evidence regarding the reliability of flux predictions for individual reactions, nor does it deliver precise predictions of absolute flux rates due to lack of information related to bidirectional reactions, metabolic cycles, or parallel pathways [22].

In order to more directly determine metabolic fluxes in the central carbon metabolism, we performed labeling experiments using [1-$^{13}$C]glucose as sole carbon source for growing Xcc. Recently, this technique [22–25] has been demonstrated to be useful for Xcc when amino acid biosynthetic pathways were identified on the basis of the label distribution in protein-derived amino acids [13]. In a subsequent study, we determined the biomass composition of Xcc B100 to employ it for FBA [21], gaining thereby fundamental data that is beneficial for metabolic flux analysis. In this study, we have used GC-MS-derived labeling data for a more detailed study of metabolic flux that also considered extracellular fluxes like glucose uptake and xanthan production. For this purpose, the demand of metabolic precursors for the Xcc biomass was determined and the mass isotopomer distributions (MIDs) of 11 amino acids were measured to facilitate $^{13}$C metabolic flux analysis. We presume this is the first application of $^{13}$C-based metabolic flux analysis for a bacterium of the genus *Xanthomonas*. Moreover, the role of central metabolic pathways was elucidated in more detail by NMR-based isotopologue profiling. Besides the Xcc B100 wild-type, a mutant strain deficient in the phosphofructokinase gene was analyzed to shed more light on metabolic processes related to glucose utilization in Xcc.

## Results and Discussion

### Establishment of the metabolic model for flux analysis based on $^{13}$C-labeled glucose

To analyze the carbohydrate flux in Xcc, a reaction network of the primary metabolism was reconstructed to establish a metabolic model for utilization with the OpenFLUX software [26]. For this purpose, data was used from genome annotation based on the sequencing of strain Xcc B100 [19]. The data considered the complete enzyme sets of three main pathways for glucose catabolism, namely the ED, PP, EMP pathways, the citrate cycle and reactions toward nucleotide sugars precursor metabolites of xanthan as a basis of the metabolic network. Information on the stoichiometry and reversibility of the reactions was adopted from the recently established large-scale metabolic network of Xcc that had been used initially to facilitate FBA modeling [21]. The biosynthetic pathways of amino acids were included as lumped reactions, meaning that unbranched sequences of multiple *in vivo* reactions were condensed to single reactions if the relevant atom compositions within these reactions did not change. Lumped reactions were included for alanine, valine, aspartate, glutamate, serine, phenylalanine, glycine, tyrosine, threonine, isoleucine, histidine, lysine, and leucine. The metabolic network including all reactions was translated into an Excel sheet (Suppl. Table 1). For $^{13}$C-flux analysis, atom transitions were defined for all reactions [26]. Furthermore, co-factors were included for all relevant reactions. Whenever possible, sets of subsequent enzymatic reactions were represented as condensed reactions when there were no changes in the atom transition. The resulting network model consisted of 79 reactions and 48 intracellular metabolites, among them 13 amino acids, plus two extracellular metabolites, namely glucose and $CO_2$ (Fig. 1, Suppl. Table 1).

To facilitate $^{13}$C-metabolic flux analysis using the OpenFLUX software [26], information on the stoichiometric demand was required in addition to the metabolic model. To determine the precursor drain toward biomass generation, the anabolic precursor demand (Table 1) was calculated based on requirements for cellular building blocks. For this purpose, the recently established biomass composition of Xcc B100 [21] was taken into account. Details are given in the methods section. The Xcc biomass is composed of about 0.49 g proteins per g cell dry weight (CDW), 0.16 g RNA per g CDW, 0.04 g DNA per g CDW, 0.13 g lipids per g CDW, and 0.033 g LPS per g CDW. The fatty acid composition for Xcc was obtained from MIDI (MIDI Sherlock TSBA40 library, version 4.10.,1/28/1999, MIDI Inc., 125 Sandy Drive, Newark, DE, 19713, USA). The data correlated well with fatty acid composition results

determined earlier for Xcc [27,28] and ranged from $C_{10:0}$ (decanoic acid) to $C_{18:1}$ (ω9-octadecenoic acid and ω7-octadecenoic acid). The most abundant fatty acid was 13-methyl tetradecanoic acid that was represented with a percentage of 23.28 %.

**GC-MS based analysis of the metabolic flux in Xcc B100**

To determine flux values for each individual reaction represented in the reconstructed metabolic network, Xcc B100 was cultivated in minimal medium containing 0.3% [1-$^{13}$C]glucose as sole carbon source. Xcc cells were harvested after 34 h, in the exponential growth phase. The cell pellet was hydrolyzed and the resulting amino acids were analyzed as *t*-butyldimethylsilyl (TBDMS) derivatives *via* GC-MS. The data obtained from GC-MS measurements were analyzed using the MeltDB software [29] to determine the mass isotopomer distributions of the amino acid derivatives. The established Xcc OpenFLUX model was applied to calculate metabolic fluxes. The glucose consumption rate had been determined as 2 mmol glucose $g^{-1}$ $h^{-1}$, the xanthan pentasaccharide production rate was 0.198 mmol $g^{1}$ $h^{1}$ and the specific growth rate was 0.05 $h^{-1}$ [21].

The metabolic model consisted of 79 reactions and 42 balanced metabolites (Suppl. Table 1). The network had 24 degrees of freedom that are called 'basis' in the OpenFLUX [26] terminology. These free independent flux parameters of the model are displayed in Suppl. Table 1. Fourteen of the OpenFLUX model bases were determined experimentally. One basis was the glucose uptake rate, which had been determined to be 2 mmol $g^{-1}$ $h^{-1}$ [21]. The glucose uptake rate was set as a reference with a value of 100 and all flux values were specified relative to this glucose uptake rate. The indicated relative flux values can be converted numerically into absolute flux values in mmol $g^{-1}$ $h^{-1}$ by dividing the given relative flux values by 50. Ten bases were derived from the anabolic precursor demand for glucose 6-phosphate, fructose 6-phosphate, ribose 5-phosphate, erythrose 4-phosphate, glyceraldehyde 3-phosphate, glycerate 3-phosphate, pyruvate, acetyl-CoA, oxaloacetate, and 2-oxoglutarate. A flux of 5.5 was determined as drain toward biomass and a flux of 7.99 was defined by the xanthan pentasaccharide unit production rate. Of the remaining eleven fluxes, seven were associated with reversible reactions. In the OpenFLUX model, for each reversible *in vivo* reaction like that catalyzed by glucose 6-phosphate isomerase, two distinct reactions are defined, one for each direction. The reverse reaction was always assigned as an additional individual basis, as reversibility of a reaction adds an additional degree of freedom to the

model [26]. Four bases were assigned to the reactions catalyzed by phosphogluconate dehydrogenase (v11), 6-phosphogluconate dehydratase (v18), isocitrate lyase (v25), and malate dehydrogenase (35), respectively, representing branching points in the metabolic network.

To facilitate the calculation of absolute fluxes within the metabolic network, mass isotopomer distributions (MIDs) were measured and included in the OpenFLUX model as additional constraints in the network besides reaction stoichiometries, reaction directions, and metabolite uptake and excretion rates. MIDs were obtained for eleven amino acids, namely for alanine, valine, threonine, glutamine, serine, phenylalanine, glycine, tyrosine, leucine, isoleucine, and asparagine (Table 2). The MIDs for the respective amino acid fragments were determined by GC-MS using selective ion monitoring (SIM) of derivatized amino acids. All MIDs were determined as mean values from three biological replicates with two technical replicates. Measured and simulated amino acid mass isotopomer fractions are compared in Table 2.

For each reaction of the metabolic network, the flux was determined in a stochastic approach based on Monte Carlo simulations, thereby providing for all reactions individual confidence intervals in addition to optimal flux values that give the best fit between the simulated and the measured data (Table 3). Subsequently, we used the Markov Chain Monte Carlo sensitivity analysis[30] to determine confidence intervals by means of OpenFlux[26] (Table 3). In addition, a non-linear algorithm[31] was applied with results that are detailed in Supplementary Table 2. Hence, two algorithms were used for confidence interval determination by means of OpenFlux[26]. The results of both computational approaches conform extensively, thereby mutually confirming their results. Calculated flux optima are not identical but always lie within the confidence intervals of the other approach.

The optimal flux values as determined by the non-linear algorithm were mapped to a graphical representation of the Xcc central carbon metabolism (Fig. 1). The visualized data clearly indicates that after its import into the cell, glucose is mainly catabolized *via* the Entner-Doudoroff (ED) pathway (81). In contrast, a low flux *via* the pentose phosphate (PP) pathway (9.42) resulted for the gluconate dehydrogenase reaction. The flux through the PP pathway was in a dimension sufficient to meet anabolic demand for biomass precursors, such as histidine and aromatic amino acids [32]. The transketolase reaction (reactions $v_{11}$/ $v_{12}$) turned out to be reversible. Besides using the ED and PP pathways, a small mass flux was apparently calculated for glucose catabolism *via* the PFK reaction of the Embden-Meyerhoff-Parnas

(EMP) pathway. Based on the GC-MS data, the Monte Carlo simulation for the phosphofructokinase reaction resulted in a confidence interval ranging from 1.22 to 6.05 (Monte Carlo analysis) and 1.7 to 2.8 for non-linear analysis for the flux *via* this reaction. Flux analysis revealed a high TCA cycle flux in Xcc. Besides being the supply for further biomass precursors, the TCA is the origin of multiple amino acids. There was apparent flux along the glyoxylate shunt, although the numerical results were not significant (Table 3). The confidence interval for the glyoxylate reactions ranged from 0 to 3.78 when calculated using the Monte Carlo Markov Chain algorithm or from 0 to 3.3 for non-linear analysis (Suppl. Table 2), respectively. The phosphogluconate dehydratase (Edd) reaction of the ED pathway, the reactions of the lower glycolysis pathway and TCA reactions had rather narrow confidence intervals. In contrast, the confidence intervals of the phosphoglucose isomerase, phosphofructokinase reactions and of the malate dehydrogenase and phosphoenolpyruvate carboxylase were rather wide.

Hence, the GC-MS based flux data demonstrated a metabolic flux originating from imported glucose mainly *via* the ED pathway and lower glycolytic reactions toward the citrate cycle. Moderate fluxes occurred in the PP pathway, the upper glycolytic pathways represented by the PFK reaction and the glyoxylate shunt, but in these cases the reliability of the data suffered from uncertainties that got apparent in substantial confidence intervals.

**Evidence from NMR-based analyses for EMP activity in Xcc B100**

$^{13}$C-Flux modeling based on GC-MS of $^{13}$C-labeled amino acids suggested a minor flux *via* glycolysis in Xcc. In order to further validate this result, we employed NMR spectroscopy to analyze in detail the positional $^{13}$C-enrichments in amino acids originating from [1-$^{13}$C]glucose that was provided as carbon source during cultivation. Data were determined comparatively for the Xcc B100 wild-type and a mutant strain derived from Xcc B100 that was devoid of the phosphofructokinase gene, *pfkA*, encoding this key enzyme of glycolysis [20]. In both strains, the major $^{13}$C-enrichments (> 38 %) were found at positions reflecting carbon flux *via* the ED pathway (Table 4, Fig. 2). More specifically, the $^{13}$C-label at C-1 of alanine clearly indicated formation of pyruvate (acting as precursor for alanine) by conversion of [1-$^{13}$C]glucose into [1-$^{13}$C]pyruvate and unlabeled glyceraldehyde phosphate *via* the intermediates [1-$^{13}$C]6-phosphogluconate and [1$^{13}$C]2-oxo-3-deoxy-6-phosphogluconate. Notably, [1-$^{13}$C]pyruvate was converted into unlabeled acetyl-CoA by decarboxylation, and,

not surprisingly, amino acids derived from intermediates of the citrate cycle were only weakly labeled. This confirmed the notion that there was no major carbon flux from pyruvate to oxaloacetate, which would have resulted in [1-$^{13}$C]-labeled oxaloacetate, aspartate, and threonine. As shown in Table 4, these specimens were not present in samples derived from the Xcc B100 wild-type and found only in low amounts (< 4 % $^{13}$C-enrichment) in samples of the PFK mutant strain. Taken together, this data indicate that the main pathway of glucose utilization is the Entner-Douderoff pathway (> 90 %) and that oxaloacetate is not formed by anaplerotic reactions.

We also noticed minor $^{13}$C-enrichment (2.9 %) at position 3 of alanine from the wild type strain. This C3-label suggested some carbon flux either *via* the non-oxidative pentose-phosphate pathway or *via* the Embden-Meyerhof-Parnas pathway (glycolysis) (Suppl. Fig. 2). By means of the initial reactions of glycolysis, [1-$^{13}$C]glucose was deduced to be converted into [3$^{13}$C]dihydroxyacetone phosphate. Catalytic action of triose phosphate isomerase results in [3$^{13}$C]glyceraldehyde phosphate. The latter species yields [3-$^{13}$C]3-phosphoglycerate, [3-$^{13}$C]phosphoenol pyruvate, [3-$^{13}$C]pyruvate, and the cognate [3-$^{13}$C]alanine (Suppl. Fig. 2). Scrambling of the $^{13}$C-label is also expected on the basis of carbon flux from [1-$^{13}$C]pyruvate produced by the ED pathway into [3,4-$^{13}$C$_1$]hexose phosphates and [1-$^{13}$C]3-phosphoglycerate *via* glycolytic cycling. Indeed, label was detected at both C-1 and C-3 of serine from the wild-type strain, reflecting a mixture of both [1-$^{13}$C]- and [3-$^{13}$C]-isotopologues for the serine precursor, 3phosphoglycerate. Presence of both serine species can therefore be taken as fingerprints for a flux contribution of the glycolytic pathway acting in both directions. Interestingly, $^{13}$C flux modeling conducted with gluconeogenic reactions did not reveal flux *via* this route. Final confirmation of the functional role of glycolysis in Xcc was elucidated on the basis of alanine and serine profiles obtained from the mutant strain lacking the phosphofructokinase gene (Table 4). In two independent labeling experiments, serine was found apparently unlabeled in the mutant strain. The label at position 3 of alanine was significantly decreased (from 2.9 to 1.8 % $^{13}$C). In conclusion, the NMR analysis confirmed the major fluxes in the OpenFLUX model calculations with the direct determination of a minor flux contribution (< 10 %) in glucose degradation by glycolysis probably including glycolytic cycling. This is consistent with the recent functional characterization of the Xcc B100 phosphofructokinase [20], thereby confirming that a complete set of EMP enzymes is available in xanthomonads.

Hence, our data show flux *via* the forward PFK reaction in Xcc, concluding that all three main pathways for glucose catabolism, the ED pathway, the PP pathway, and the EMP pathway, are active in Xcc. The availability and parallel activity of three catabolic pathways is an unusual feature. In particular, it seemed unusual that the ED pathway is the prevalent route for glucose catabolization while glycolysis is available. Considering efficiency of ATP production, glycolysis is the most efficient pathway for glucose catabolism. This leads to the question why Xcc predominantly uses the Entner-Doudoroff pathway instead of glycolysis. The kinetic constants determined for the Xcc PFK clearly reflect a minor processivity of that enzyme. Actually, the PFK had some non-canonical features as it uses pyrophosphate as cosubstrate and had no indications for allosteric regulation contrasting in these aspects to conventional ATP-dependent PFKs. Flux *via* glycolysis may be limited due to this low processivity of the Xcc PFK. Based on profound analysis of other bacteria it is quite doubtful whether regulation at the transcriptional level might compensate for the low enzymatic PFK activity to a degree that evokes metabolic effects on the level of flux distribution [33,34]. A hypothesis to elucidate a prevalent role of the ED pathway in glucose catabolization assumes that organisms that use the ED pathway are not dependent on living in energy-limited environments so that efficiency in ATP generation is not significantly advantageous for them [35]. This was first discussed for *Zymomonas mobilis*, a Gram-negative proteobacterium that constitutively uses the ED pathway. It was found in warm climates associated with plants harboring a high sugar content in their xylem sap [36]. Xanthomonads are plant pathogenic bacteria and Xcc initially grows in xylem sap of *Brassicaceae* before it invades other plant tissues in the course of infection. GC-MS analysis revealed in xylem sap of the Xcc host plant *Brassica olerace* diverse sugars and organic acids [37,38]. But in particular when plant defense is overpowered by the pathogen attack and xanthomonads advance from the xylem toward surrounding tissues, a wealth of metabolic resources from the host plant is likely to get available to them. Xanthomonads have diverse degradative exoenzymes available [39] plus a wide range of import systems in both cellular membranes [19,40] to scavenge such resources toward their central metabolism. Under such circumstances, tremendous viable bacterial titers are observed for Xcc *in planta* [41]. Hence, akin to *Z. mobilis*, utilizing the ED pathway for glucose catabolism could be an adaptation to a nutrient-rich environment. However, when seeing carbon utilization in a wider perspective it may be meaningful that Xcc imports the carbon sources sucrose, malate, citrate and amino acids prior to importing fructose and glucose when these compounds are available in parallel [42]. Thus, Xcc metabolism is not likely to be optimized toward growth on glucose as carbon source. Likewise, diauxic growth of

*Pseudomonas* on glucose and succinate revealed that succinate is preferred as carbon source and genes encoding glucose catabolizing enzymes are repressed in this organism until succinate is consumed [43,44].

Still, rather few bacteria are known to use the ED pathway, the PP pathway, and the EMP pathway in parallel as *Roseobacter denitrificans* [45]. For some of these and for additional bacteria that highly employ the ED pathway there is quantitative data for the individual contributions of these pathways to glucose utilization (Table 5). A genomic analysis indicated a particular prevalence of the ED pathway in aerobic bacteria [56]. The ED pathway generates NADPH as reducing equivalents instead of NADH that is generated by the EMP pathway. While NADPH provides reducing equivalents for biosynthetic reactions, biosynthesis of ED pathway enzymes is expected to require substantial fewer metabolic resources to achieve the same glucose conversion rate as the EMP pathway [56]. Moreover, recent experimental findings from a taxonomically close proteobacterium remind of another advantage the ED pathway provides. Chavarría et al. have analyzed the effect of artificially enabling EMP activity in *Pseudomonas putida*, an organism that like Xcc mainly uses the ED pathway to catabolize glucose[57]. They introduced a transgenic phosphofructokinase from *Escherichia coli* into *P. putida*. The transgenic *P. putida* cells became highly sensitive to hydrogen peroxide; thereby pointing to the role of the ED pathway in NADPH generation, as NADPH is utilized not only for biosynthetic reactions but also for the detoxication of reactive oxygen species (ROS)[58]. Likewise, the introduction of a transgenic pyrophosphate-dependent phosphofructokinase did not result in noticeable EMP activity in *Z. mobilis*, possibly due to interference with redox balancing[59]. As deduced for the engineered *P. putida* cells [57], support for effective detoxication of ROS by ED pathway activity may be a key advantage also for Xcc, in particular in pathogenic interactions with plants.

It is tempting to compare the flux data provided by this $^{13}C$ metabolic flux analysis to predictions determined recently by FBA for the central metabolism of the same Xcc wild-type strain B100 [21]. Both complementary techniques [60] provide similar results in the case of Xcc. Yet, results from this study provide a potential to further enhance the FBA model in a subtle way by including experimentally determined fluxes as constraints for individual reactions [61]. Such combining of the strengths of both approaches could not only obtain a clearer perspective of the Xcc metabolism. Conducting isotopically non-stationary $^{13}C$-labeling experiments might be a promising next step to study the dynamics of the Xcc carbohydrate metabolism in more detail [62–64] besides extending the Xcc metabolic model to fully consider

co-factor balancing. In particular, it would be of interest to obtain an initial grasp of the dynamic *in planta* metabolism of phytopathogenic bacteria like xanthomonads. Thereby, perhaps not only from an evolutionary point of view, it may become interesting to compare the flow of reducing equivalents in the interaction of plant and bacterial pathogen with data emerging for phototrophic bacteria [65]. Likewise, based on a deeper understanding of metabolic fluxes in Xcc, it may be possible to elucidate for xanthomonads the presence of "flux sensors" [34] that were recently found to regulate metabolism in response to actually occurring metabolic fluxes in *E. coli* cells.

## Experimental

### Strains and molecular biology

Strains studied in this work are the *Xanthomonas campestris* pv. campestris B100 wild-type [19,66] and a mutant strain B100Δ*pfkA* wherein the *pfkA* gene encoding a well-conserved phosphofructokinase was deleted [21]. Xcc cells were grown in rich TY medium containing 5 g of tryptone, 3 g of yeast extract, and 0.7 g of $CaCl_2$ per l [67]. When required, the antibiotic streptomycin (Sm) was added to the media in a concentration of 800 µg/ml. Pre-cultures were cultivated in the modified minimal medium XMD [21] supplemented with 0.3 % glucose. XMD medium contained per liter 1 g of $K_2HPO_4 \cdot 3\ H_2O$, 1 g of $KH_2PO_4$, 0.6 g of $KNO_3$, 0.25 g of $MgSO_4 \cdot 7\ H_2O$ , 0.1 g of $CaCl_2 \cdot 2\ H_2O$, and 0.2 µg of $FeCl_3$. To start cultivation for the labeling experiment, pre-culture was used as inoculum in a volume of one tenth of the final volume, resulting in a minor contamination of unlabeled biomass and glucose. For the labeling experiment, Xcc cells were grown in XMD minimal medium with 0.3% [1-$^{13}$C]glucose (99% $^{13}$C enrichment, Euriso Top GmbH, Saarbrücken, Germany). Xcc cells were incubated in Erlenmeyer flasks at 30°C, shaking at 180 rpm. After 34 h, bacteria were harvested in the exponential growth phase (OD 0.8) by centrifugation at 20,000 × g, washed with isotonic buffer saline (0.9% NaCl), frozen in liquid nitrogen and finally lyophilized as described previously[13]. The lyophilized cell pellet was treated and subjected to GC-MS and NMR analysis as described below.

### GC-MS and fluxome analysis

For the GC-MS-based metabolic flux analysis, the lyophilized cell pellet was hydrolyzed and the derived amino acids were converted into *t*-butyldimethylsilyl (TBDMS) derivatives as

described previously [47,68]. Briefly, 4 to 5 mg of the cell pellet was hydrolyzed with 250 µl 6 M HCl and incubated at 110°C for 4 hours. The hydrolysates were neutralized by addition of NaOH and filtered using a 0.2µm centrifuge filter device (Ultrafree MC, Merck Millipore, MA, USA). Samples were dried by a stream of nitrogen and derivatized at 80°C by addition of 250 µl *N*,*N*-dimethylformamide (Carl Roth, Karlsruhe, Germany) with 0.1 % (v/v) pyridine and 50 µl *N*-methyl-*tert*-butyldimethylsilyl-trifluoracetamide (Macherey-Nagel, Düren, Germany) for 60 min. For the GC-MS analysis, 1 µl of sample was injected to a GC-MS G-CQ system (Thermo Finnigan, Waltham, MA, US). GC-MS conditions were used as described previously [69]. Samples were first measured in scan mode to check for other sample components. Subsequently, the relative fractions of different mass isotopomers ($M_0$, $M_1$, …, $M_n$) were measured in triplicates with selective ion monitoring (SIM). The resulting data was converted to cdf format using the Xcalibur software (Thermo Finnigan, Waltham, MA, USA). The data was imported to the MeltDB software [29] that has been recently enhanced and extended [70]. Thereby, targeted fragments of metabolites from the Xcc metabolism were verified based on retention times and mass values expected from the SIM measurements. Chromatographic peak detection was performed in MeltDB and the mass isotopomers at the apex of identified chromatographic peaks were extracted from raw measurement data. For flux analysis, it is important to correct MS raw data for the contribution of naturally abundant isotopes [71]. Specific interactive software is available for such purposes [72], but to streamline data processing respective functionality has been integrated into MeltDB [29]. By means of this added functionality, the mass isotope distribution (MID) was corrected for naturally occurring isotopes when using the MeltDB tool "13C flux analysis" and exported as Excel worksheets.

**Establishment of the metabolic network and calculation of metabolic fluxes**

A model for the Xcc B100 central carbohydrate metabolism that includes atom transitions (Suppl. Table 1) was built with Excel for the $^{13}C$ flux modeling software OpenFLUX [26]. Carbon metabolite requirements for cell growth (Table 1) were calculated [73] from the experimentally determined biomass composition of Xcc [21] by using known anabolic pathways [21]. Co-factors were added to all relevant reactions as recently conducted for another organism [74], thereby using NADH for modeling also for NADP-depending reactions. The Xcc biomass is composed of 0.49 g per g CDW proteins, 0.16 g per g CDW RNA, 0.04 g per g CDW DNA, 0.13 g per g CDW lipids, and 0.033 g per g CDW LPS. The fatty acid composition was

obtained from MIDI (MIDI Sherlock TSBA40 library, version 4.10.,1/28/1999, MIDI, Inc.,125 Sandy Drive, Newark, DE, 19713, USA, Xanthomonas-campestris-campestris). For substrate consumption, xanthan production, and specific growth rates had been experimentally determined previously as 2 mmol glucose $g^{-1}$ $h^{-1}$, 0.198 mmol pentasaccharide $g^{-1}$ $h^{-1}$, and 0.05 $h^{-1}$, respectively [21], and were now applied as inputs for the model [75]. Outputs of biomass precursors were determined by multiplication of the anabolic demand by the specific growth rate [75]. The glucose uptake in the model was set to 100 to obtain relative flux values for glucose uptake. The carbon flux at each step of the pathway was determined by assuming that metabolite pools did not vary within steady-state cultures. The corrected MIDs obtained from MeltDB were included in the model. For visualization, the predicted fluxes were imported into ProMeTra [76] and the values were mapped onto the metabolic network of Xcc (Fig. 1).

The intracellular fluxes were determined by metabolite and isotopomer balancing *via* the reaction network regarding the atom transitions of the reactions. The unknown free fluxes were calculated using a nonlinear least-squares fitting procedure. Starting from random numbers, it calculates MID and flux values from the available data by variation of the free fluxes in an attempt to minimize the deviation between experimental and simulated MIDs [26,77]. Establishment of the metabolic network and flux calculations were performed using the OpenFLUX [26] modeling software which is based on elementary metabolite units [78]. In this work, 55 mass isotopomer fractions were regarded (Table 2). To account for measurement errors, MS analysis considered data from three biological replicates with at least two technical replicates. The reversible reactions of the lower glycolysis reactions glyceraldehyde 3-phosphate dehydrogenase (EC 1.2.1.12, *gapA*), phosphoglycerate kinase (EC 2.7.2.3, *pgk*), phosphoglycerate mutase (EC 5.4.2.1, *gpm1*, *gpm2*), and phosphopyruvate hydratase (EC 4.2.1.11, *eno1*, *eno2*) were transformed to unidirectional reactions, since they are supposed to exclusively facilitate glycolytic reactions when grown on glucose as sole carbon source [79–81]. Parameter estimation was performed ten times with 50 iterations. The goodness of fit was evaluated with a $\chi^2$-test regarding the obtained minimal sum of squares. Statistical analysis was conducted using a Monte Carlo approach [30]. Experimental errors encountered when mean values were determined in the GC-MS measurements were included as random errors in the analysis, thereby assuming a normal distribution of measurement errors in previously obtained mean values. With the Markov Chain Monte Carlo approach [30] a 95% confidence interval was determined for the variable values of those fluxes that are not predefined by the

precursor drain (Table 3). Results were confirmed by a second, independent approach using a non-linear approach developed by Antoniewicz et al [31] implemented in the OpenFlux software (Supplementary Table 2 and Fig. 1).

**NMR-based $^{13}$C-isotopologue profiling of amino acids from *X. campestris* pv. campestris wilde-type and a PFK deletion mutant**

For NMR analysis, about 200 mg of Xcc cells (dry weight) were hydrolyzed and processed as described previously [13,82] . Briefly, amino acids from the acidic cell hydrolysates were purified by cation exchange chromatography. Fractions containing specific amino acids were subsequently dried under reduced pressure. The residues were dissolved in $D_2O$/DCl (pH 1) and subjected to quantitative NMR spectroscopy using a 500 MHz Bruker instrument equipped with a dual $^{13}$C-$^{1}$H probe head. Positional $^{13}$C-enrichments were calculated from the NMR signal integrals as described before [13,82,83]. For each strain, two independent biological replicates were analyzed.

## Conclusions

To our knowledge, the $^{13}C$ metabolic flux analysis of Xcc presented here is the first application of this experimental approach to determine metabolic rates in the *Xanthomonadaceae* clade, which includes a wide range of plant pathogens, several of which are agriculturally relevant being causal agents of plant diseases that lead to severe losses of important crops [1]. Our study combines two complementary techniques, GC-MS-based $^{13}C$ metabolic flux analysis and NMR spectroscopy-based $^{13}C$-isotopologue profiling [84–86], both tracing [1-$^{13}C$]glucose-derived metabolic intermediates, to obtain a more detailed view on the Xcc central metabolism and its key enzymatic interconversions. The consistent findings of both approaches are mutually affirmative. Likewise, vast agreement with results from a recent FBA analysis [21] does not only widely confirm the FBA predictions but is also a good indication for the reliability of this $^{13}C$ metabolic flux analysis. Extensive accordance with outcomes from earlier studies that indicated prevalence of the ED pathway in Xcc on the basis of other techniques [11,12,14,17,18] further confirms the applicability of $^{13}C$ metabolic flux analysis to xanthomonads. Hence, this study clearly indicates that xanthomonads utilize glucose mainly *via* the ED pathway, in minor amounts *via* the PP and EMP pathways. Adjusting previous conceptions, xanthomonads use the EMP pathway in minor extent as determined by our flux measurement *in vivo*. However, EMP fluxes *via* the EMP pathway were low. Physiological interpretation of these results is challenging, as glucose might play a minor role as C-source in natural habitats of xanthomonads. Yet, a deeper understanding of metabolic fluxes originating from glucose as intended to be initiated by this first $^{13}C$ metabolic flux analysis of *Xanthomonas* is important, not only due to the paramount role of glucose in experimental approaches aiming at fundamental insights into the metabolism, but also due to the prevalent use of glucose as carbon source in large-scale industrial cultivation of Xcc for xanthan production [6,9]. Future research might expand this work by applying instationary flux analysis or including co-factor balancing, which might further increase the precision of the flux estimation for some of the reactions and reveal additional fundamental properties of the Xcc metabolism.

## Conflict of interest

No conflicts of interest exist.

**Acknowledgements**

We thank Tobias Fürch for helpful discussions related to the analysis of GC-MS and MID data and in particular for his induction to selective ion monitoring (SIM) measurements.

This work was supported by grant SPP 1316 awarded by Deutsche Forschungsgemeinschaft (DFG) and by the GenoMik Plus program of the German Federal Ministry of Education and Research (BMBF). Sarah Schatschneider was supported by Hans Böckler Foundation, by the CLIB graduate cluster and by a scholarship of Bielefeld University.

## Figure Legends

**Figure 1. *In vivo* carbon flux distribution of *X. campestris* pv. campestris B100 as determined by GC-MS based metabolic flux analysis.** The fluxes calculated based on $^{13}C$ GC-MS measurements are mapped to the metabolic network reconstructed for Xcc B100. Numerical data of fluxes relative to a glucose uptake rate set as 100 are indicated in the vicinity of the individual reactions that are symbolized by arrows. Arrow widths are proportional to the relative fluxes determined. The biomass precursor drains (BM) are displayed in grey and symbolized by dashed arrows. Flux values were calculated using a non-linear algorithm. The data is given in Suppl. Table 2, reaction IDs are documented in Suppl. Fig. 1. The main flux was determined through the Entner-Doudoroff pathway. Since the glucose uptake rate was determined to be 2 mmol $g^{-1}$ $h^{-1}$, the indicated relative flux values can be converted to absolute flux rates in the unit mmol $g^{1}$ $h^{1}$ by dividing the flux values by 50. The metabolic network underlying the model includes the Embden-Meyerhof-Parnas pathway, the pentose phosphate pathway, the Entner-Doudoroff pathway, gluconeogenesis, the tricaboxylic acid cycle, biosynthesis of xanthan precursors, and lumped reactions for the amino acids biosyntheses of alanine (Ala), valine (Val), aspartate (Asp), glutamate (Glu), serine (Ser), phenylalanine (Phe), glycine (Gly), tyrosine (Tyr), threonine (Thr), tryptophan (Trp), isoleucine (Ile), histidine (His), lysine (Lys) and leucine (Leu), Minor fluxes contributing to biomass generation with numerical flux values less than 0.1 were not included to avoid cluttering the diagram. Glc-6P, glucose 6-phosphate; Fru-6P, fructose 6-phosphate; Fru-1,6$P_2$, fructose 1,6-bisphosphate; P-5P, pentose 5-phosphate; S-7P, sedoheptulose 7--phosphate; E-4P, erythrose 4-phosphate, GAP, glyceraldehyde 3-phosphate; DHAP, dihydroxyacetone phosphate; GA3P, 3-Phosphoglycerate; PEP, phosphoenolpyruvate; Pyr, pyruvate; Ac-CoA, acetyl-CoA; CitA, citrate; αk-GlA, α-ketoglutarate (2-oxoglutarate); SucA, succinate; FumA, fumarate, MalA, malate; OAA, oxaloacetate; $CO_2$, carbon dioxide.

**Figure 2. Comparative NMR analysis of $^{13}$C-labeled metabolites of *X. campestris* pv. campestris B100 related to glycolysis.** NMR analysis was performed for the Xcc B100 wild-type (A) and for the B100Δ*pfkA* deletion mutant deficient in phosphofructokinase, a key enzyme of the Embden-Meyerhof-Parnas pathway (glycolysis) (B). A grey dot symbolizes $^{13}$C label of imported [1-$^{13}$C]glucose. Green dots indicate $^{13}$C label which was derived from [1-$^{13}$C]glucose metabolized *via* glycolysis while red dots reflect label derived from [1-$^{13}$C]glucose metabolized through the Entner-Doudoroff pathway. More than 90 percent of [1-$^{13}$C]glucose-derived label originated from the Entner-Doudoroff pathway. Poor label quantities indicate that glycolysis and the pentose phosphate pathway collectively contribute less than 10 % to glucose catabolism. The natural abundance of $^{13}$C labeling is 1.1%. This should be considered when low levels of $^{13}$C labeling are observed. Data related to $^{13}$C labels was known for the imported [1-$^{13}$C]glucose and determined experimentally for alanine, glycine, and serine (Table 4); digits giving the measurement results. Labels at the respective intermediate metabolites are interpolations which indicate minimal labeling required for obtaining the measured amino acid labels *via* the known biosynthetic pathways.

**References**


1. R. P. Ryan, F.-J. Vorhölter, N. Potnis, J. B. Jones, M.-A. Van Sluys, A. J. Bogdanove, and J. M. Dow, *Nat. Rev. Microbiol.*, 2011, **9**, 344–355.
2. J. G. Vicente and E. B. Holub, *Mol. Plant Pathol.*, 2013, **14**, 2–18.
3. S. N. Aslam, M.-A. Newman, G. Erbs, K. L. Morrissey, D. Chinchilla, T. Boller, T. T. Jensen, C. De Castro, T. Ierano, A. Molinaro, R. W. Jackson, M. R. Knight, and R. M. Cooper, *Curr Biol*, 2008, **18**, 1078–1083.
4. G. Dunger, C. G. Garofalo, N. Gottig, B. S. Garavaglia, M. C. P. Rosa, C. S. Farah, E. G. Orellano, and J. Ottado, *Mol. Plant Pathol.*, 2012, **13**, 865–876.
5. M. H. Yun, P. S. Torres, M. El Oirdi, L. A. Rigano, R. Gonzalez-Lamothe, M. R. Marano, A. P. Castagnaro, M. A. Dankert, K. Bouarab, and A. A. Vojnov, *Plant Physiol.*, 2006, **141**, 178–187.
6. F. García-Ochoa, V.E . Santos, J. . Casas, and E. Gómez, *Biotechnol Adv.*, 2000, **18**, 549–579.
7. F. García-Ochoa, E. Gomez, A. Alcon, and V. E. Santos, *Bioprocess Biosyst Eng*, 2013, **36**, 911–925.
8. F. Létisse, N. D. Lindley, and G. Roux, *Biotechnol. Prog.*, 2003, **19**, 822–827.
9. G. Hublik, in *Polymer Science: A Comprehensive Reference*, eds. K. Matyjaszewski and M. Möller, Elsevier, Amsterdam, 2012, pp. 221–229.
10. G.-T. Lu, Z.-J. Yang, F.-Y. Peng, Y.-N. Tan, Y.-Q. Tang, J.-X. Feng, D.-J. Tang, Y.-Q. He, and J.-L. Tang, *Microbiology,* 2007, **153**, 4284–4294.
11. C. Whitfield, I. W. Sutherland, and R. E. Cripps, *J Gen Microbiol*, 1982, **128**, 981–985.
12. F. Létisse, P. Chevallereau, J.-L. Simon, and N. Lindley, *J. Biotechnol.*, 2002, **99**, 307–317.
13. S. Schatschneider, F.-J. Vorhölter, C. Rückert, A. Becker, W. Eisenreich, A. Pühler, and K. Niehaus, *Mol. Genet. Genomics*, 2011, **286**, 247–259.
14. A. C. Zagallo and C. H. Wang, *J. Bacteriol.*, 1967, **93**, 970–975.
15. R. M. Hochster and H. Katznelson, *Can. J. Biochem. Physiol.*, 1958, **36**, 669–689.
16. J.-C. Portais and A.-M. Delort, *FEMS Microbiol Rev.*, 2002, **26**, 375–402.
17. S.-Y. Kim, B.-M. Lee, and J.-Y. Cho, *Biotechnol. Lett.*, 2010, **32**, 527–531.
18. P. Pielken, K. L. Schimz, L. Eggeling, and H. Sahm, *Can. J. Microbiol.*, 1988, **34**, 1333–1337.
19. F.-J. Vorhölter, S. Schneiker, A. Goesmann, L. Krause, T. Bekel, O. Kaiser, B. Linke, T. Patschkowski, C. Rückert, J. Schmid, V. K. Sidhu, V. Sieber, A. Tauch, S. A. Watt, B. Weisshaar, A. Becker, K. Niehaus, and A. Pühler, *J. Biotechnol.*, 2008, **134**, 33–45.
20. M. Frese, S. Schatschneider, J. Voss, F.-J. Vorhölter, and K. Niehaus, *Arch. Biochem. Biophys.*, 2014, **546**, 53–63.
21. S. Schatschneider, M. Persicke, S. A. Watt, G. Hublik, A. Pühler, K. Niehaus, and F.-J. Vorhölter, *J. Biotechnol.*, 2013.
22. W. Wiechert, *Metab. Eng.*, 2001, **3**, 195–206.
23. W. Eisenreich, T. Dandekar, J. Heesemann, and W. Goebel, *Nat. Rev. Microbiol.*, 2010, **8**, 401–412.
24. U. Sauer, *Mol Syst Biol*, 2006, **2**, 62.
25. C. Wittmann, *Microb Cell Fact.*, 2007, **6**, 6.
26. L.-E. Quek, C. Wittmann, L. Nielsen, and J. Krömer, *Microbial Cell Factories*, 2009, **8**, 25.
27. L. Vauterin, P. Yang, and J. Swings, *Int. J. Syst. Bacteriol.*, 1996, **46**, 298–304.
28. P. Yang, L. Vauterin, M. Vancanneyt, J. Swings, and K. Kersters, *Systematic and Applied Microbiology*, 1993, **16**, 47–71.
29. H. Neuweger, S. P. Albaum, M. Dondrup, M. Persicke, T. Watt, K. Niehaus, J. Stoye, and A. Goesmann, *Bioinformatics*, 2008, **24**, 2726–2732.

30. V. Kadirkamanathan, J. Yang, S. A. Billings, and P. C. Wright, *Bioinformatics*, 2006, **22**, 2681–2687.
31. M. R. Antoniewicz, J. K. Kelleher, and G. Stephanopoulos, *Metab. Eng.*, 2006, **8**, 324–337.
32. T. Fuhrer and U. Sauer, *J Bacteriol.*, 2009, **191**, 2112–2121.
33. K. Kochanowski, U. Sauer, and V. Chubukov, *Curr. Opin. Biotechnol.*, 2013.
34. K. Kochanowski, B. Volkmer, L. Gerosa, B. R. Haverkorn van Rijsewijk, A. Schmidt, and M. Heinemann, *Proc. Natl. Acad. Sci. U.S.A.*, 2013, **110**, 1130–1135.
35. T. Conway, *FEMS Microbiol Lett.*, 1992, **103**, 1–28.
36. J. Swings and J. De Ley, *Bacteriol. Rev.*, 1977, **41**, 1–46.
37. N. Fernandez-Garcia, M. Hernandez, J. Casado-Vela, R. Bru, F. Elortza, P. Hedden, and E. Olmos, *Plant Cel Environ*, 2011, **34**, 821–836.
38. T. Dugé de Bernonville, L. D. Noël, M. SanCristobal, S. Danoun, A. Becker, P. Soreau, M. Arlat, and E. Lauber, *FEMS Microbiol. Ecol.*, 2014.
39. A. C. R. da Silva, J. A. Ferro, F. C. Reinach, C. S. Farah, L. R. Furlan, R. B. Quaggio, C. B. Monteiro-Vitorello, M. A. Van Sluys, N. F. Almeida, L. M. C. Alves, A. M. do Amaral, M. C. Bertolini, L. E. A. Camargo, G. Camarotte, F. Cannavan, J. Cardozo, F. Chambergo, L. P. Ciapina, R. M. B. Cicarelli, L. L. Coutinho, J. R. Cursino-Santos, H. El-Dorry, J. B. Faria, A. J. S. Ferreira, R. C. C. Ferreira, M. I. T. Ferro, E. F. Formighieri, M. C. Franco, C. C. Greggio, A. Gruber, A. M. Katsuyama, L. T. Kishi, R. P. Leite, E. G. M. Lemos, M. V. F. Lemos, E. C. Locali, M. A. Machado, A. M. B. N. Madeira, N. M. Martinez-Rossi, E. C. Martins, J. Meidanis, C. F. M. Menck, C. Y. Miyaki, D. H. Moon, L. M. Moreira, M. T. M. Novo, V. K. Okura, M. C. Oliveira, V. R. Oliveira, H. A. Pereira, A. Rossi, J. A. D. Sena, C. Silva, R. F. de Souza, L. A. F. Spinola, M. A. Takita, R. E. Tamura, E. C. Teixeira, R. I. D. Tezza, M. Trindade dos Santos, D. Truffi, S. M. Tsai, F. F. White, J. C. Setubal, and J. P. Kitajima, *Nature*, 2002, **417**, 459–463.
40. G. Déjean, S. Blanvillain-Baufumé, A. Boulanger, A. Darrasse, T. Dugé de Bernonville, A.-L. Girard, S. Carrére, S. Jamet, C. Zischek, M. Lautier, M. Solé, D. Büttner, M.-A. Jacques, E. Lauber, and M. Arlat, *New Phytol.*, 2013, **198**, 899–915.
41. H. G. Wiggerich and A. Pühler, *Microbiology*, 2000, **146 ( Pt 5)**, 1053–1060.
42. T. F. Watt, M. Vucur, B. Baumgarth, S. A. Watt, and K. Niehaus, *J. Biotechnol.*, 2009, **140**, 59–67.
43. D. N. Collier, P. W. Hager, and P. V. Phibbs Jr., *Res Microbiol.*, 1996, **147**, 551–561.
44. F. Rojo, *FEMS Microbiol. Rev.*, 2010, **34**, 658–684.
45. K.-H. Tang, X. Feng, Y. J. Tang, and R. E. Blankenship, *PLoS ONE*, 2009, **4**, e7233.
46. T. Fuhrer, E. Fischer, and U. Sauer, *J Bacteriol.*, 2005, **187**, 1581–1590.
47. T. Fürch, M. Preusse, J. Tomasch, H. Zech, I. Wagner-Döbler, R. Rabus, and C. Wittmann, *BMC Microbiol.*, 2009, **9**, 209.
48. S. Sudarsan, S. Dethlefsen, L. M. Blank, M. Siemann-Herzberg, and A. Schmid, *Appl. Environ. Microbiol.*, 2014.
49. A. Berger, K. Dohnt, P. Tielen, D. Jahn, J. Becker, and C. Wittmann, *PLoS ONE*, 2014, **9**, e88368.
50. N. Gunnarsson, U. H. Mortensen, M. Sosio, and J. Nielsen, *Mol Microbiol.*, 2004, **52**, 895–902.
51. I. Borodina, C. Schöller, A. Eliasson, and J. Nielsen, *Appl. Environ. Microbiol.*, 2005, **71**, 2294–2302.
52. L. He, Y. Xiao, N. Gebreselassie, F. Zhang, M. R. Antoniewicz, Y. J. Tang, and L. Peng, *Biotechnol. Bioeng.*, 2014, **111**, 575–585.
53. E. Fischer, N. Zamboni, and U. Sauer, *Analytical Biochemistry*, 2004, **325**, 308–316.
54. T. Bartek, B. Blombach, S. Lang, B. J. Eikmanns, W. Wiechert, M. Oldiges, K. Nöh, and S. Noack, *Appl. Environ. Microbiol.*, 2011, **77**, 6644–6652.

55. A. Swarup, J. Lu, K. C. DeWoody, and M. R. Antoniewicz, *Metab. Eng.*, 2014, **24C**, 173–180.
56. A. Flamholz, E. Noor, A. Bar-Even, W. Liebermeister, and R. Milo, *PNAS*, 2013, **110**, 10039–10044.
57. M. Chavarría, P. I. Nikel, D. Pérez-Pantoja, and V. de Lorenzo, *Environ Microbiol*, 2013, **15**, 1772–1785.
58. J. A. O'Brien, A. Daudi, V. S. Butt, and G. P. Bolwell, *Planta*, 2012, **236**, 765–779.
59. R. R. Chen, M. Agrawal, and Z. Mao, *Appl. Biochem. Biotechnol.*, 2013, **170**, 805–818.
60. X. Chen, A. P. Alonso, D. K. Allen, J. L. Reed, and Y. Shachar-Hill, *Metabolic Engineering*, 2011, **13**, 38–48.
61. J. Schellenberger, R. Que, R. M. T. Fleming, I. Thiele, J. D. Orth, A. M. Feist, D. C. Zielinski, A. Bordbar, N. E. Lewis, S. Rahmanian, J. Kang, D. R. Hyduke, and B. Ø. Palsson, *Nat Protoc*, 2011, **6**, 1290–1307.
62. A. Buchholz, J. Hurlebaus, C. Wandrey, and R. Takors, *Biomol. Eng.*, 2002, **19**, 5–15.
63. M. Hörl, J. Schnidder, U. Sauer, and N. Zamboni, *Biotechnol. Bioeng.*, 2013, **110**, 3164–3176.
64. K. Nöh, K. Grönke, B. Luo, R. Takors, M. Oldiges, and W. Wiechert, *J. Biotechnol.*, 2007, **129**, 249–267.
65. K.-H. Tang, Y. J. Tang, and R. E. Blankenship, *Front Microbiol*, 2011, **2**.
66. B. Hötte, I. Rath-Arnold, A. Pühler, and R. Simon, *J. Bacteriol.*, 1990, **172**, 2804–2807.
67. J. E. Beringer, *J Gen Microbiol*, 1974, **84**, 188–198.
68. C. Wittmann, M. Hans, and E. Heinzle, *Anal. Biochem.*, 2002, **307**, 379–382.
69. T. Fürch, R. Hollmann, C. Wittmann, W. Wang, and W.-D. Deckwer, *Bioprocess Biosyst Eng*, 2007, **30**, 47–59.
70. N. Kessler, H. Neuweger, A. Bonte, G. Langenkämper, K. Niehaus, T. W. Nattkemper, and A. Goesmann, *Bioinformatics*, 2013, **29**, 2452–2459.
71. W. A. Van Winden, C. Wittmann, E. Heinzle, and J. J. Heijnen, *Biotechnol. Bioeng*, 2002, **80**, 477–479.
72. P. Millard, F. Letisse, S. Sokol, and J.-C. Portais, *Bioinformatics*, 2012, **28**, 1294–1296.
73. J. L. Ingraham, *Growth of the bacterial cell*, Sinauer Associates,, Sunderland, Mass. :, c1983.
74. J. Nocon, M. G. Steiger, M. Pfeffer, S. B. Sohn, T. Y. Kim, M. Maurer, H. Rußmayer, S. Pflügl, M. Ask, C. Haberhauer-Troyer, K. Ortmayr, S. Hann, G. Koellensperger, B. Gasser, S. Y. Lee, and D. Mattanovich, *Metab. Eng.*, 2014, **24C**, 129–138.
75. M. Cocaign-Bousquet, A. Guyonvarch, and N. D. Lindley, *Appl Environ Microbiol*, 1996, **62**, 429–436.
76. H. Neuweger, M. Persicke, S. P. Albaum, T. Bekel, M. Dondrup, A. T. Hüser, J. Winnebald, J. Schneider, J. Kalinowski, and A. Goesmann, *BMC Systems Biology*, 2009, **3**, 82.
77. C. Wittmann and E. Heinzle, *Appl. Environ. Microbiol.*, 2002, **68**, 5843–5859.
78. M. R. Antoniewicz, J. K. Kelleher, and G. Stephanopoulos, *Metab Eng*, 2007, **9**, 68–86.
79. S. O. Han, M. Inui, and H. Yukawa, *Microbiology*, 2007, **153**, 2190–2202.
80. M.-K. Oh, L. Rohlin, K. C. Kao, and J. C. Liao, *J. Biol. Chem.*, 2002, **277**, 13175–13183.
81. L. Peng and K. Shimizu, *Appl Microbiol Biotechnol*, 2003, **61**, 163–178.
82. W. Eisenreich, B. Schwarzkopf, and A. Bacher, *J. Biol. Chem.*, 1991, **266**, 9622–9631.
83. W. Eisenreich and A. Bacher, *Phytochemistry*, 2007, **68**, 2799–2815.
84. K. Al Zaid Siddiquee, M. J. Arauzo-Bravo, and K. Shimizu, *Appl. Microbiol. Biotechnol.*, 2004, **63**, 407–417.
85. M. Li, P. Y. Ho, S. Yao, and K. Shimizu, *J. Biotechnol.*, 2006, **122**, 254–266.
86. L. Peng, M. J. Arauzo-Bravo, and K. Shimizu, *FEMS Microbiol. Lett.*, 2004, **235**, 17–23.

1

**Table 1**
Anabolic precursor demand for biomass synthesis in *Xanthomonas campestris* pv. campestris B100 in µmol/g dry cell mass

| Precursor(µmol/g) | | Amount | G6P | F6P | R5P | E4P | GAP | PGA | PEP | PYR | AcCoA | OAA | AKG | NADPH |
|---|---|---|---|---|---|---|---|---|---|---|---|---|---|---|
| Ala | | 631 | | | | | | | | 1 | | | | 1 |
| Arg | | 224 | | | | | | | | | | | 1 | 4 |
| Asx | | 296 | | | | | | | | | | 1 | | 1 |
| Cys | | 149 | | | | | | 1 | | | | | | 5 |
| Glx | | 354 | | | | | | | | | | | 1 | 1 |
| Gly | | 376 | | | | | | 1 | | | | | | 1 |
| His | | 120 | | | 1 | | | | | | | | | 1 |
| Ile | | 166 | | | | | | | | 1 | | 1 | | 5 |
| Leu | | 340 | | | | | | | | 2 | 1 | | | 2 |
| Lys | | 190 | | | | | | | | 1 | | 1 | | 4 |
| Met | | 9 | | | | | | | | | | 1 | | 8 |
| Phe | | 149 | | | | 1 | | | 2 | | | | | 2 |
| Pro | | 94 | | | | | | | | | | | 1 | 3 |
| Ser | | 232 | | | | | | 1 | | | | | | 1 |
| Thr | | 347 | | | | | | | | | | 1 | | 3 |
| Trp | | 17 | | | 1 | 1 | | | 1 | | | | | 2 |
| Tyr | | 188 | | | | 1 | | | 2 | | | | | 2 |
| Val | | 275 | | | | | | | | 2 | | | | 2 |
| **Protein** | | 4155 | 0 | 0 | 137 | 354 | 0 | 757 | 690 | 1586 | 340 | 1007 | 672 | 8564 |
| ATP | | 112 | | | 1 | | | 1 | | | | | | 1 |
| GTP | | 138 | | | 1 | | | 1 | | | | | | |
| CTP | | 119 | | | 1 | | | | | | | 1 | | 1 |
| UTP | | 100 | | | 1 | | | | | | | 1 | | 1 |
| RNA | | | 0 | 0 | 469 | 0 | 0 | 250 | 0 | 0 | 0.00 | 219 | 0 | 331 |
| dATP | | 21 | | | 1 | | | 1 | | | | | | 2 |
| dGTP | | 37 | | | 1 | | | 1 | | | | | | 1 |
| dCTP | | 42 | | | 1 | | | | | | | 1 | | 2 |
| dTTP | | 22 | | | 1 | | | | | | | 1 | | 3 |
| **DNA** | | | 0 | 0 | 122 | 0 | 0 | 58 | 0 | 0 | 0.00 | 64 | 0 | 229 |
| Glycerol-3-phosphate | | 215 | | | | | 1 | | | | | | | 1 |
| Serine | | 215 | | | | | | 1 | | | | | | 1 |
| 10:0 (0.92%) | 0.92 | | | | | | | | | | 5 | | | 8 |
| 11:0 ISO (3.69%) | 3.69 | | | | | | | | | 2 | 4 | | | 8 |
| 11:0 ISO 3OH (2.25%) | 2.25 | | | | | | | | | 2 | 4 | | | 8 |
| 12:0 3OH (3.01%) | 3.01 | | | | | | | | | | 6 | | | 10 |
| 14:0 ISO (0.34%) | 0.34 | | | | | | | | | 2 | 6 | | | 12 |
| 14:0 (1.35%) | 1.35 | | | | | | | | | | 7 | | | 12 |
| 13:0 ISO 3OH (3.27%) | 3.27 | | | | | | | | | 2 | 6 | | | 11 |
| 15:1 ISO F (0.38%) | 0.38 | | | | | | | | | 2 | 6 | | | 12 |
| 15:0 ISO(23.28%) | 23.28 | | | | | | | | | 2 | 6 | | | 13 |
| 15:0 ANTEISO (13.46%) | 13.46 | | | | | | | | | 2 | 6 | | | 13 |
| 15:0 (1.44%) | 1.44 | | | | | | | | | | 7 | | | 13 |
| 16:0 ISO (2.33%) | 2.33 | | | | | | | | | 2 | 7 | | | 14 |
| 16:1 w9c (2.13%) | 2.13 | | | | | | | | | 2 | 7 | | | 13 |
| 16:0 (5.48%) | 5.48 | | | | | | | | | | 8 | | | 14 |
| ISO 17:1 w9c (7.32%) | 7.32 | | | | | | | | | 2 | 8 | | | 14 |
| 17:0 ISO (7.15%) | 7.15 | | | | | | | | | 2 | 8 | | | 15 |
| 17:0 ANTEISO (0.82%) | 0.82 | | | | | | | | | 2 | 8 | | | 15 |
| 17: 1 w8c (1.32%) | 1.32 | | | | | | | | | | 8 | | | 14 |
| 18: 1 w9c (0.54%) | 0.54 | | | | | | | | | | 9 | | | 15 |
| 18: 1 w7c (0.47%) | 0.47 | | | | | | | | | | 9 | | | 15 |
| 17:0 ISO 3OH (0.35%) | 0.35 | | | | | | | | | 2 | 8 | | | 15 |
| | 81.30 | | | | | | | | | | | | | |
| ***Average Fatty Acids*** | | *429* | | | | | | | | *1.6426* | *6.52* | | | *12.793* |
| **Lipids** | | | 0 | 0 | 0 | 0 | 215 | 215 | 0 | 704.66 | 2797.52 | 0 | 0 | 5488.192 |
| UDP-Glucose | | 19 | 1 | | | | | | | | | | | |
| CDP(Ethanolamine) | | 28 | | | | | | 1 | | | | | | 1 |
| OH-Myristic acid | | 28 | | | | | | | | | 7.00 | | | 11 |
| C:14 | | 28 | | | | | | | | | 7.00 | | | 12 |
| (CMP)KDO | | 28 | | | 1 | | | | 1 | | | | | |
| (NDP)Heptose | | 28 | 1.50 | | | | | | | | | | | -4 |
| (TDP)Glucosamine | | 19 | | 1 | | | | | | | | | | |
| **LPS** | | | 61 | 19 | 28 | 0 | 0 | 28 | 28 | 0 | 392.00 | 0 | 0 | 560 |
| UDP-N-Acetylglucosamine | | 27.6 | | 1 | | | | | | | 1.00 | | | |
| UDP-N-Acetylmuramic acid | | 27.6 | | 1 | | | | | 1 | | 1.00 | | | 1 |
| Alanine | | 55.2 | | | | | | | | 1 | | | | 1 |
| Diaminopimelate | | 27.6 | | | | | | | | 1 | | 1 | | 4 |
| Glutamate | | 27.6 | | | | | | | | | | | 1 | 1 |
| **Peptidoglycan** | | | 0 | 55.2 | 0 | 0 | 0 | 0 | 27.6 | 82.8 | 55.20 | 27.6 | 27.6 | 220.8 |
| Glucose | | 154 | 1 | | | | | | | | | | | |
| **Glycogen** | | | 154 | 0 | 0 | 0 | 0 | 0 | 0 | 0 | 0.00 | 0 | 0 | 0 |
| Serine | | 48.5 | | | | | | 1 | | | | | | 1 |
| C1-Units | | | 0 | 0 | 0 | 0 | 0 | 48.5 | 0 | 0 | 0.00 | 0 | 0 | 48.5 |
| Ornithine equivalents | | 59.3 | | | | | | | | | | | 1 | 3 |
| Polyamines | | | 0 | 0 | 0 | 0 | 0 | 0 | 0 | 0 | 0.00 | 0 | 59.3 | 177.9 |
| **TOTAL** | **376** | **6210** | **215** | **74.2** | **755.7** | **353.8** | **215** | **1357** | **746** | **2373** | **3584.81** | **1317** | **759** | **15619** |

**Table 2**
Mass isotopomer fractions of amino acids from the cell protein of *Xanthomonas campestris* pv. campestris B100

| Amino Acid | | Mass isotopomers | | |
|---|---|---|---|---|
| | | $M_0$ | $M_1$ | $M_2$ |
| Alanine | Calc | 0.334 | 0.497 | 0.125 |
| 260 | Exp | 0.334 | 0.496 | 0.126 |
| Alanine | Calc | 0.756 | 0.174 | 0.070 |
| 232 | Exp | 0.756 | 0.174 | 0.070 |
| Valine | Calc | 0.320 | 0.487 | 0.137 |
| 288 | Exp | 0.318 | 0.488 | 0.140 |
| Valine | Calc | 0.721 | 0.192 | 0.073 |
| 260 | Exp | 0.718 | 0.193 | 0.075 |
| Threonine | Calc | 0.603 | 0.249 | 0.112 |
| 404 | Exp | 0.612 | 0.248 | 0.106 |
| Threonine | Calc | 0.620 | 0.244 | 0.109 |
| 376 | Exp | 0.616 | 0.246 | 0.110 |
| Aspartate | Calc | 0.602 | 0.248 | 0.113 |
| 418 | Exp | 0.613 | 0.247 | 0.107 |
| Aspartate | Calc | 0.725 | 0.198 | 0.076 |
| 302 | Exp | 0.721 | 0.196 | 0.083 |
| Glutamate | Calc | 0.591 | 0.254 | 0.115 |
| 432 | Exp | 0.596 | 0.253 | 0.114 |
| Serine | Calc | 0.639 | 0.229 | 0.107 |
| 390 | Exp | 0.646 | 0.228 | 0.101 |
| Serine | Calc | 0.665 | 0.229 | 0.106 |
| 362 | Exp | 0.662 | 0.229 | 0.106 |
| Phenylalanine | Calc | 0.667 | 0.226 | 0.085 |
| 336 | Exp | 0.671 | 0.227 | 0.080 |
| Phenylalanine | Calc | 0.728 | 0.197 | 0.076 |
| 302 | Exp | 0.735 | 0.189 | 0.075 |
| Glycine | Calc | 0.760 | 0.170 | |
| 246 | Exp | 0.759 | 0.172 | |
| Glycine | Calc | 0.829 | 0.171 | |
| 218 | Exp | 0.828 | 0.172 | |
| Tyrosine | Calc | 0.574 | 0.262 | 0.120 |
| 466 | Exp | 0.568 | 0.265 | 0.122 |
| Tyrosine | Calc | 0.728 | 0.197 | 0.076 |
| 302 | Exp | 0.725 | 0.199 | 0.076 |
| Leucine | Calc | 0.697 | 0.209 | 0.077 |
| 274 | Exp | 0.699 | 0.207 | 0.077 |
| Histidine | Calc | 0.366 | 0.367 | 0.178 |
| 440 | Exp | 0.364 | 0.366 | 0.177 |

**Table 3**
Probability distributions of confidence intervals for individual reaction rates using a Monte Carlo approach: Calculated optimum of free fluxes and the associated 95% confidence interval

| Reaction equation | Parameters [a] | optValue [b] | lower CI [c] | upperCI [d] | Gene name | Enzyme | EC number |
|---|---|---|---|---|---|---|---|
| GLC6P = F6P/F6P = GLC6P | v(2)-v(3) | 3.85 | 1.9 | 8.82 | *pgi* | Glc6P-Isomerase | 5.3.1.9 |
| F6P + PPi = F16BP | v(7) | 2.7 | 1.22 | 6.05 | *pfkA* | Phosphofructokinase | 2.7.1.11 |
| GLC6P = 6PG + NADH | v(10) | 90.4 | 85.5 | 96.2 | *zwf/ gnl* | glucose-6-phosphate dehydrogenase / 6-phosphogluconolactonase | 1.1.1.49 / 3.1.1.31 |
| 6PG = P5P + CO2 + NADH | v(11) | 9.42 | 6.98 | 12.2 | *gnd* | phosphogluconate dehydrogenase | 1.1.1.44 |
| P5P + P5P = S7P + G3P/S7P + G3P = P5P + P5P | v(12)-v(13) | 2.2 | 1.39 | 3.12 | *tkt* | Transketolase 1 | 2.2.1.1 |
| S7P + G3P = E4P + F6P/E4P + F6P = S7P + G3P | v(14)-v(15) | 2.2 | 1.39 | 3.12 | *tal* | Transaldolase | 2.2.1.2 |
| E4P + P5P = F6P + G3P/F6P + G3P = E4P + P5P | v(16)-v(17) | 0.0281 | -0.782 | 0.942 | *tkt* | Transketolase 2 | 2.2.1.1 |
| GLC6P = G3P + PYR | v(18) | 81 | 78.5 | 84 | *eda edd* | 6P-Gluconate-dehydratase | 4.2.1.12 |
| G3P = 3PG + ATP + NADH | v(19) | 85.4 | 81.4 | 88.7 | *gapA, pgk* | GAPDH | 1.2.1.12 |
| 3PG = PEP | v(20) | 75.9 | 72 | 79.3 | *gpm1, gpm2, eno1, eno2* | Phosphoglycerate-mutase/phosphopyruvate hydratase | 5.4.2.1 / 4.2.1.11 |
| PEP = PYR + ATP | v(21) | 59.9 | 25.5 | 66.6 | *pykA* | Pyruvate Kinase | 2.7.1.40 |
| PYR + ATP = PEP | v(22) | 0.236 | 0 | 1.1 | *ppsA* | Phosphoenolpyruvate synthase | 2.7.9.2 |
| PYR = ACCOA + CO2 + NADH | v(23) | 132 | 130 | 135 | *pdhABC* | Pyruvate-dehydrogenase | 1.2.4.1 |
| ACCOA + OAA = CIT | v(24) | 112 | 111 | 113 | *gltA* | Citrate synthase | 2.3.3.1 |
| CIT = GLYOXY + 0.5 SUC + 0.5 SUC | v(25) | 1.29 | 0 | 3.78 | *aceA* | Isocitrate lyase | 4.1.3.1 |
| ACCOA + GLYOXY = MAL | v(26) | 1.29 | 0 | 3.78 | *aceB* | Malate synthase | 2.3.3.9 |
| CIT = AKG + CO2 + NADH | v(27) | 111 | 107 | 113 | *icd1, icd2, acnB* | Aconitate Hydratase/Isocitrate dehydrogenase | 4.2.1.3 / 1.1.1.41 |
| AKG = SUCCOA + CO2 + NADH | v(28) | 106 | 103 | 108 | *sucA* | Oxoglutarate dehydrogenase | 1.2.4.2 |
| SUCCOA = 0.5 SUC + 0.5 SUC + ATP | v(29) | 106 | 103 | 108 | *sucB* | Dihydrolipoyllysine-residue succinyltransferase | 2.3.1.61 |
| SUC = FUM + FADH2 | v(30) | 107 | 106 | 108 | *sdhABCD* | Succinate dehydrogenase | 1.3.5.1 |
| FUM = MAL | v(31) | 107 | 106 | 108 | *fumBC* | Fumarate hydratase | 4.2.1.2 |
| MAL = OAA + NADH | v(32) | 107 | 77.5 | 108 | mdh | Malate dehydrogenase | 1.1.1.37 |
| PEP + CO2 = OAA/ OAA = PEP + CO2 | v (34)-v(33) | 12.7 | 10.2 | 42.9 | *ppc* | Phosphoenolpyruvate carboxylase | 4.1.1.31 |
| MAL = PYR + CO2 + NADH | v (35) | 0 | 0 | 29 | *maeB* | Malate dehydrogenase | 1.1.1.40 |

[a]) Relevant reaction rate/ reaction rate tested
[b]) Optimum value for the flux parameters calculated from the free flux parameter
[c]) Lower boundary of associated confidence interval
[d]) Upper boundary of associated confidence interval

**Table 4**

$^{13}$C-enrichments observed for amino acids from *X. campestris* pv. campestris B100 labeled with [1$^{13}$C]glucose

| WT [a] | | | | B100Δ*pfkA1* [b] | | | | B100Δ*pfkA2* [b] | | | |
|---|---|---|---|---|---|---|---|---|---|---|---|
| Amino acid | Position | Chemical Shift in ppm | %$^{13}$C | Amino acid | Position | Chemical Shift in ppm | %$^{13}$C | Amino acid | Position | Chemical Shift in ppm | %$^{13}$C |
| **Alanine** | **1** | **173.5** | **46.6** | **Alanine** | **1** | **173.1** | **38.4** | **Alanine** | **1** | **173.1** | **38.3** |
| | **2** | **49.2** | **1.1** | | **2** | **48.9** | **1.1** | | **2** | **48.9** | **1.1** |
| | **3** | **15.4** | **2.9** | | **3** | **15.3** | **1.9** | | **3** | **15.3** | **1.8** |
| Serine | 1 | 170.7 | 6.2 | Serine | 1 | 170.4 | 1.8 | Serine | 1 | 170.5 | 1.8 |
| | 2 | 56.4 | 1.1 | | 2 | 54.8 | 1.1 | | 2 | 54.9 | 1.1 |
| | 3 | 59.5 | 5.9 | | 3 | 59.3 | 1.3 | | 3 | 59.4 | 1.2 |
| Lysine | 1 | 172.9 | 18.7 | Lysine | 1 | 172.9 | 25.8 | Lysine | 1 | 172.7 | 22.4 |
| | 2 | 53.5 | 1.1 | | 2 | 53.3 | 1.3 | | 2 | 53.2 | 1.0 |
| | 3 | 29.4 | 7.8 | | 3 | 29.4 | 1.7 | | 3 | 29.4 | 1.6 |
| | 4 | 21.3 | 3.2 | | 4 | 21.3 | 3.6 | | 4 | 21.3 | 3.3 |
| | 5 | 26.2 | 2 | | 5 | 26.3 | 1.5 | | 5 | 26.3 | 1.5 |
| | 6 | 28.9 | 1.3 | | 6 | 38.9 | 1.1 | | 6 | 39.9 | 1.1 |
| Arginine | 1 | – | – | Arginine | 1 | 172.5 | 2.4 | Arginine | 1 | 172.7 | 2.8 |
| | 2 | 53.4 | 1.1 | | 2 | 53 | 1.1 | | 2 | 53.2 | 1.4 |
| | 3 | 27.1 | 1.8 | | 3 | 27 | 1.2 | | 3 | 27 | 1.4 |
| | 4 | 23.7 | 2.1 | | 4 | 23.5 | 1.4 | | 4 | 23.7 | 1.6 |
| | 5 | 40.3 | 1.3 | | 5 | 40.3 | 1.1 | | 5 | 40.3 | 1.1 |
| | 6 | 156.7 | 15.5 | | 6 | 156.6 | 15.1 | | 6 | 156.6 | 15.8 |
| Aspartate | 1 | 169.8 | 1.1 | Aspartate | 1 | 171.8 | 1.9 | Aspartate | 1 | 171.9 | 1.9 |
| | 2 | 52.8 | 3.3 | | 2 | 49.4 | 1.1 | | 2 | 49.5 | 1.1 |
| | 3 | 33.9 | 1.4 | | 3 | 33.7 | 1.1 | | 3 | 33.8 | 1.2 |
| | 4 | 171.5 | 1.7 | | 4 | 173.2 | 2.6 | | 4 | 173.3 | 2.7 |
| Glutamate | 1 | 169.3 | 1.6 | Glutamate | 1 | 170.7 | 1.1 | Glutamate | 1 | 170.8 | 1.1 |
| | 2 | 52.6 | 1.3 | | 2 | 52.2 | 1.3 | | 2 | 52.3 | 1.2 |
| | 3 | 25.0 | 1.1 | | 3 | 24.8 | 1.5 | | 3 | 24.9 | 1.4 |
| | 4 | 29.5 | 1.3 | | 4 | 29.4 | 1.6 | | 4 | 29.4 | 1.4 |
| | 5 | 172.3 | 2.4 | | 5 | 176.3 | 1.2 | | 5 | 176.3 | 1.2 |
| Threonine | 1 | 171.1 | 1.3 | Threonine | 1 | 170.7 | 3.5 | Threonine | 1 | 170.9 | 3.9 |
| | 2 | 58.9 | 1.1 | | 2 | 58.6 | 1.1 | | 2 | 58.7 | 1.1 |
| | 3 | 65.3 | 1.3 | | 3 | 65.2 | 1.2 | | 3 | 65.2 | 1.1 |
| | 4 | 18.9 | 2.8 | | 4 | 18.9 | 2.6 | | 4 | 18.9 | 2.5 |
| Glycine | 1 | 171.7 | 1.9 | Glycine | 1 | 170.2 | 1.5 | Glycine | 1 | 170.2 | 1.7 |
| | 2 | 49.8 | 1.1 | | 2 | 40.2 | 1.1 | | 2 | 40.2 | 1.1 |
| Tyrosine | 1 | 169.0 | 6.7 | Tyrosine | 1 | 173.7 | n.a | Tyrosine | 1 | 173.2 | 1.6 |
| | 2 | 35.8 | 1.1 | | 2 | 55.5 | 1.1 | | 2 | 55.4 | 1.1 |
| | 3 | 21.9 | 1.6 | | 3 | 35.1 | 1.4 | | 3 | 35.1 | 1.3 |
| | 4 | 127.8 | 1.9 | | 4 | 126.3 | 1.1 | | 4 | 126.3 | 1.1 |
| | 5/9 | – | – | | 5/9 | 130.7 | 1.3 | | 5/9 | 130.7 | 1.1 |
| | 6/8 | 117.0 | 1.9 | | 6/8 | 115.8 | 2.2 | | 6/8 | 115.8 | 2.1 |
| | 7 | 155.3 | 8.1 | | 7 | 154.8 | 1.2 | | 7 | 154.9 | 1.2 |
| Leucine | 1 | 169.3 | 4.9 | | | | | Leucine | 1 | 169.5 | 1.1 |
| | 2 | 46.1 | 1.3 | | | | | | 2 | 51.9 | 6.0 |
| | 3 | 35.7 | 1.1 | | | | | | 3 | 35.7 | 2.2 |
| | 4 | 28.7 | 3.9 | | | | | | 4 | 23.9 | 4.5 |
| | 5 | 24.6 | 1.8 | | | | | | 5 | 20.7 | 7.9 |
| | 6 | 24.3 | 1.2 | | | | | | 6 | 21.6 | 7.7 |

a) Data taken from Schatschneider et al., 2011

b) Individual biological replicate measurements of the B100Δ*pfkA* mutant strain deficient in the phosphofructokinase gene

**Table 5**
Metabolic flux in catabolic key pathways determined for bacterial species with Entner-Doudoroff pathway activities grown on glucose

| Organism | ED flux [a] | PP flux [a] | EMP flux [a] | Reference |
|---|---|---|---|---|
| *Zymomonas mobilis* (DSMZ 424) | 100 | — [b] | — [b] | [44] |
| *Rhodobacter sphaeroides* ATH 2.4.1 (DSMZ 158) | 100 | 0 | 0 | [44] |
| *Dinoroseobacter shibae* DFL12 | > 99 | < 1 | < 1 | [45] |
| *Phaeobacter gallaeciensis* DSMZ 17395 | > 99 | < 1 | < 1 | [45] |
| *Pseudomonas putida* KT2440 | 97 | 3 | — [b] | [46] |
| *Sinorhizobium meliloti* TAL 380 (DSMZ 1981) | 95 | 0 | — [b] | [44] |
| *P. fluorescens* 52-1C | 91 | 2 | — [b] | [44] |
| *P. aeruginosa* PAO1 | 87 | 11 | 0 [c] | [47] |
| Uropathogenic *P. aeruginosa* isolates | 91 | 7 | 2 [c] | [47] |
| *Agrobacterium tumefaciens* C58 | 86 | 0 | — [b] | [44] |
| *Xanthomonas campestris* pv. campestris B100 | 81 | 9 | 2 | This study |
| *Nonomuraea* sp. ATCC 39727 | 59 | 40 | 24 | [48] |
| *Streptomyces tenebrarius* TD507 | 42 | 5 | 44 | [49] |
| *Escherichia coli* DH1 | 2 | 26 | 71 | [50] |
| *E. coli* MG1655 | 4 | 22 | 73 | [51] |
| *Corynebacterium glutamicum* ATCC 13032 [d] | — [b] | 69 | 27 | [52] |
| *Thermus thermophilus* HB8 [d] | 0 | 0 | 98 | [53] |

[a] Molar net fluxes as percentage of glucose uptake / glucose consumption rate. Measurement errors were ignored as different analytical methods were applied.
[b] This pathway was considered absent based on literature data.
[c] Incomplete EMP pathway due to lacking phosphofructokinase reaction.
[d] Included for the purpose of comparison.

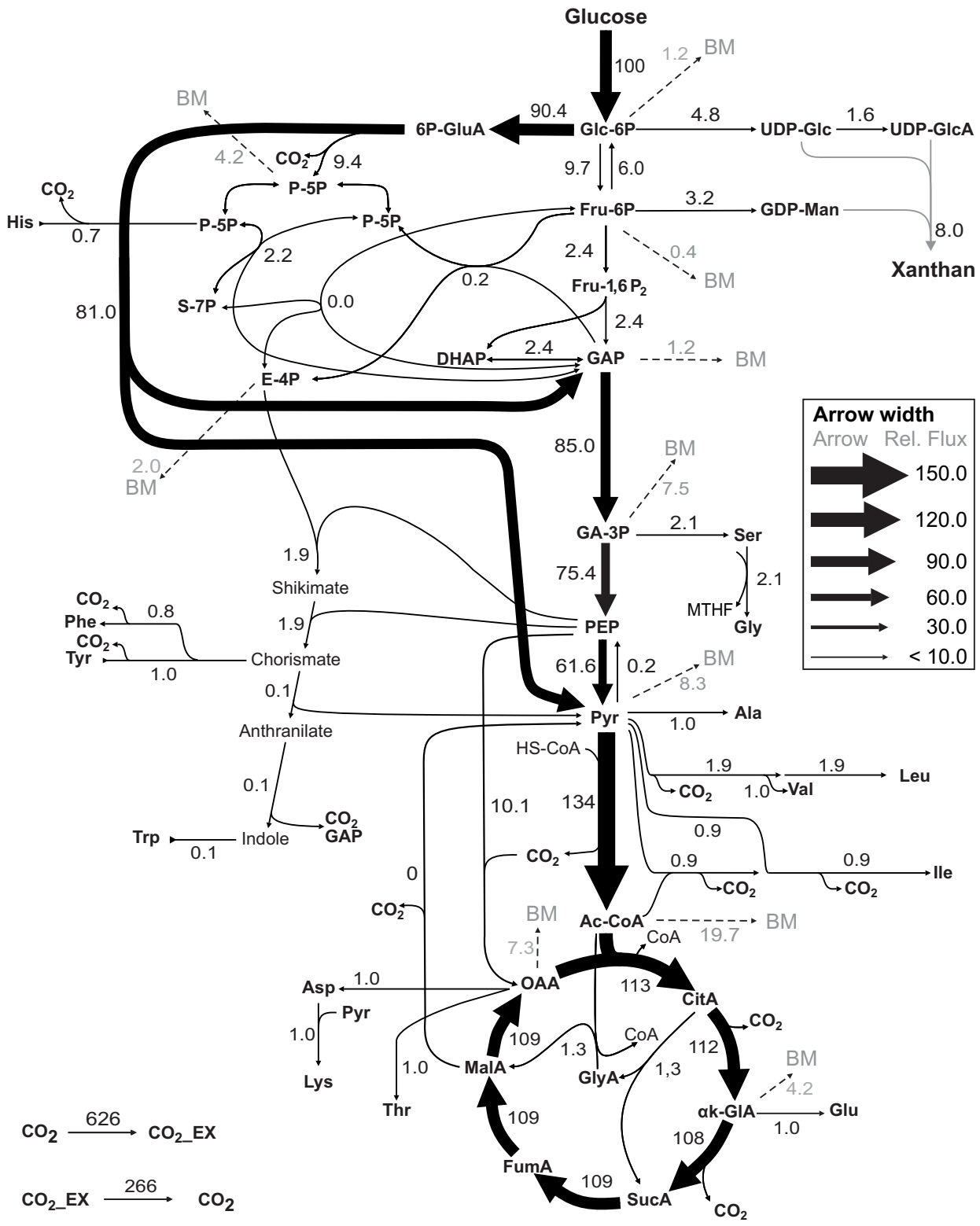


Figure 1

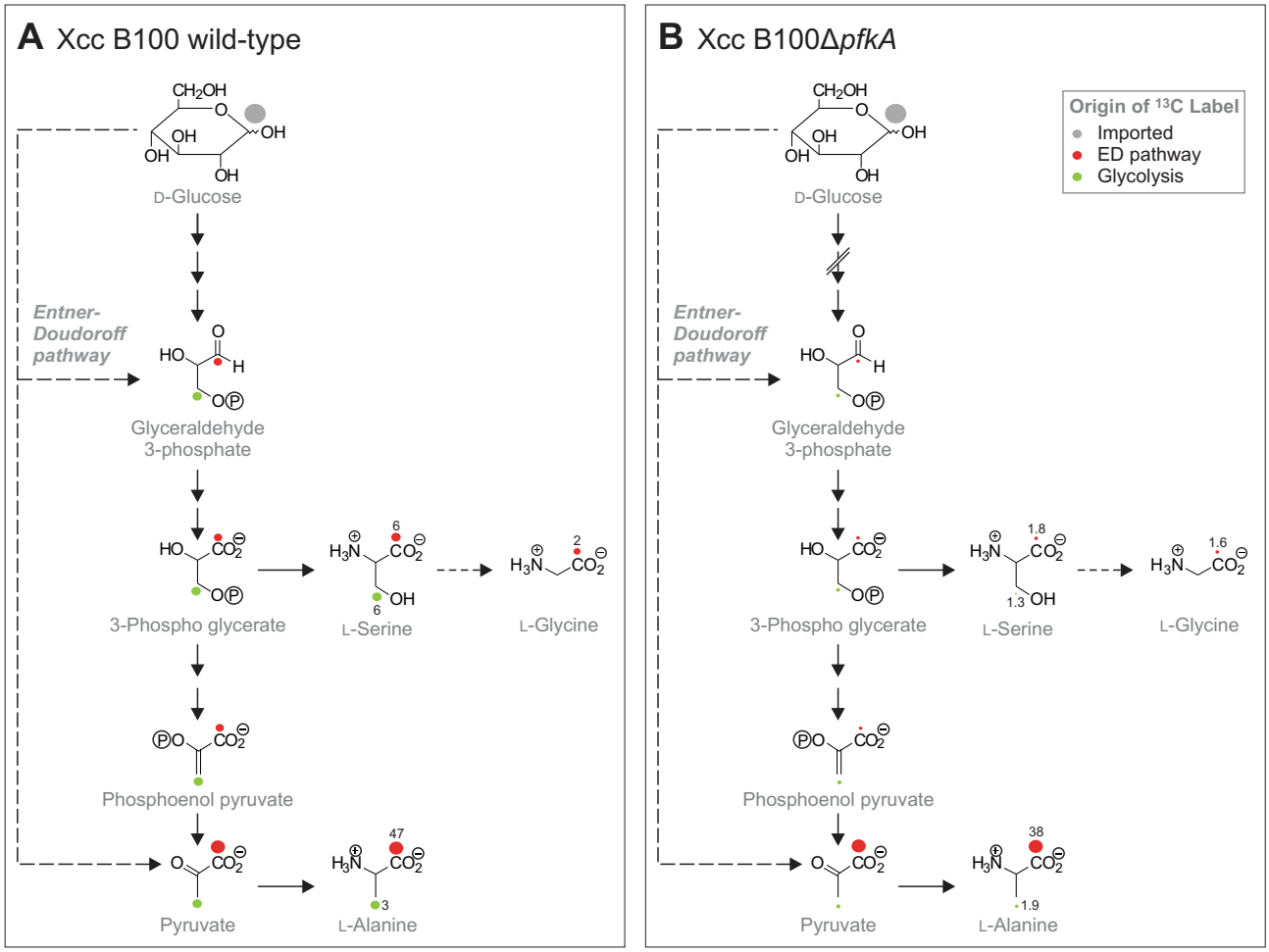


Figure 2